Structural, energetic, and electronic trends in low-dimensional late-transition-metal systems

C. H. Hu,[1,*] C. Chizallet,[2] H. Toulhoat,[3] and P. Raybaud[2,†]

[1]*Direction Chimie et Physico-Chimie Appliquées, IFP, 1 et 4 Avenue de Bois-Préau, 92852 Rueil-Malmaison Cedex, France*

[2]*Direction Catalyse et Séparation, IFP-Lyon, Rond-point de l'échangeur de Solaize, BP 3, 69360 Solaize, France*

[3]*Direction Scientifique, IFP, 1 et 4 Avenue de Bois-Préau, 92852 Rueil-Malmaison Cedex, France*

(Received 28 July 2008; revised manuscript received 12 March 2009; published 14 May 2009)

Using first-principles calculations, we present a comprehensive investigation of the structural trends of low dimensionality late 4*d* (from Tc to Ag) and 5*d* (from Re to Au) transition-metal systems including 13-atom clusters. Energetically favorable clusters not being reported previously are discovered by molecular-dynamics simulation based on the simulated annealing method. They allow a better agreement between experiments and theory for their magnetic properties. The structural periodic trend exhibits a nonmonotonic variation of the ratio of square to triangular facets for the two rows, with a maximum for Rh_{13} and Ir_{13}. By a comparative analysis of the relevant energetic and electronic properties performed on other metallic systems with reduced dimensionalities such as four-atom planar clusters, one-dimensional (1D) scales, double scales, 1D cylinders, monatomic films, two and seven layer slabs, we highlight that this periodic trend can be generalized. Hence, it appears that 1D-metallic nanocylinders or 1D-double nanoscales (with similar binding energies as TM_{13}) also favor square facets for Rh and Ir. We finally propose an interpretation based on the evolution of the width of the valence band and of the Coulombic repulsions of the bonding basins.

DOI: 10.1103/PhysRevB.79.195416 PACS number(s): 61.46.Bc, 73.22.−f, 36.40.Cg, 36.40.Mr

I. INTRODUCTION

Over the past two decades, metallic nanoparticles and clusters have been extensively studied owing to the potential technological applications in catalysis,[1,2] magnetic nanostructures,[3] and photonic devices.[4] A better understanding of the structural and energetic properties of such systems becomes crucial. Much effort has been invested on small metal clusters of up to about 20 atoms due to their size-dependent structural and electronic properties.[5–8] As a first magic number shell corresponding to the face-centered-cubic (fcc) close-packed icosahedral and cuboctahedral structures, the 13-atom transition-metal (TM_{13}) clusters have recently attracted much interest. However, it is still difficult for experimental techniques, such as photoelectron spectroscopy (PES), transmission electron microscopy (TEM), and extended X-ray absorption fine structure (EXAFS), to determine morphologies and sizes of those clusters since they may be reshaped under experimental conditions even after deposition on an oxide support.[8–10] The different cluster morphologies, intimately related to their electronic structure, can however directly affect their physical and chemical properties.

Recently, first-principles calculations based on density-functional theory (DFT) have been widely used to investigate the geometries of small metal clusters, especially of TM_{13} clusters. The early theoretical calculations indicated that the stable atomic structure is an icosahedron (ICO) [Fig. 1(a)] for Ni_{13},[11] Rh_{13},[12,13] and Pd_{13} (Refs. 14 and 15) clusters, and a cuboctahedron (CUB) [Fig. 1(b)] for Pt_{13} (Ref. 6) and Au_{13}.[16] However, more recent electronic structure calculations have shown that TM_{13} clusters prefer lower-symmetry structures.[17–31] For example, Chang and Chou[17] found that a buckled biplanar (BBP) [Fig. 1(c)] structure with a C_{2v} symmetry is more stable than the close-packed ICO and CUB structures for the elements with more than half-filled *d* shells. Futschek *et al.*[18,19] found a new biplanar (NBP) [Fig. 1(d)] structure energetically favorable for Pd_{13} and Pt_{13}. In addition, a top-capped simple cubic (TCSC) [Fig. 1(e)] isomer was found to be preferred for Ru_{13}, Rh_{13}, and Ir_{13}.[20,32] More recently, based on a first-principles simulated annealing (SA) method,[33] more stable structures for Pt_{13} [called hereafter "capped biplanar triangle (CBPT)," Fig. 1(f)] and Rh_{13} [called "side-capped simple cubic (SCSC)," Fig. 1(g)] was reported by Wang and Johnson[21] and for Ru_{13} by Li *et al.*[22] [called "disordered SCSC (dSCSC)," Fig. 1(h)]. On the basis of these previous theoretical low-lying structures, it can be observed that TM_{13} clusters may exhibit a wide structural diversity.

However, one challenging question is whether one can identify a general periodic trend in morphologies for the series of late 4*d* and 5*d* TM_{13} owing to the periodic change in *d*-band filling. Sun *et al.*[29] very recently addressed this topic using SA methods or the "taboo search in descriptor space (TSDS)"[34] algorithm for the systematic investigation of the preferred geometry, over a wide range of elements, among others 4*d* and 5*d* transition metals. They observe a stronger propensity of bonds to form 90° angles for rather *d* rich elements ($d_n, 5 \leq n \leq 8$), which they assign to the localized character of the bonding as a convolution effect of half *d* band filling and screened nuclear charge.

The present work is devoted to the rationalization of such trends for late transition metals by *d* shell filling and dimensionality considerations. A systematic investigation of the morphology of late TM_{13} clusters is performed, using DFT calculations and a simulated annealing method. We report some structures which improve the understanding of experimentally measured magnetic properties. We will show how the simulation of complementary systems of increasing dimensionality (TM_4, scales, double scales, cylinders, and slabs of various width) leads to a rationale of structural and electronic trends observed for TM_{13} clusters.

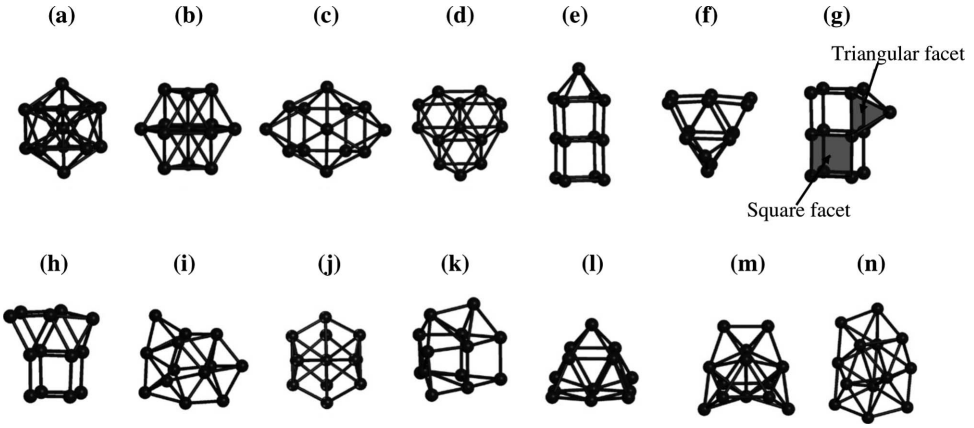

FIG. 1. Atomic structures of the isomers considered in the present work for late 4*d* and 5*d* TM_{13} clusters: (a) Icosahedron (ICO); (b) Cuboctaedron (CUB); (c) Buckled bi-planar (BBP); (d) new biplanar (NBP); (e) Top-capped simple-cubic (TCSC); (f) Capped Biplanar Triangle (CBPT); (g) side-capped simple cubic (SCSC); (h) distorted SCSC (dSCSC); (i) Au_SA; (j) Tc_SA; (k) Pt_SA; (l) Pt_SA2; (m) Pd_SA; (n) Ag_SA. "_SA" means the isomer is from first-principles molecular dynamics based on simulated annealing method.

II. METHODS AND MODELS

Calculations are performed within the DFT by using a plane-wave method as implemented in the Vienna *ab initio* Simulation Package (VASP).[35,36] The exchange-correlation functional was treated using the PW91 form of the generalized gradient approximation[37] and the electron-ion interaction was described by the projector augmented wave scheme.[38,39] The interpolation formula of Vosko *et al.*[40] was used for the correlation part of the exchange-correlation functional. The maximal kinetic-energy cutoffs plus 30% as provided in the pseudopotential database were used, which guarantees that the energy is converged down to a few meV. Order 1 Methfessel-Paxton smearing (σ=0.1 eV) was applied. With spin-polarized (SP) calculations, we scanned the space of possible magnetic structures, except for some competing isomers, where fixed spin moment modes were considered, as suggested by Ref. 41. The valence density of states (DOS) $N(\varepsilon)$ was calculated by carefully adjusting Wigner-Seitz radii of each metallic element and system to recover the expected total number of $(s+d)$ electrons of the metallic system.

The TM_{13} clusters were optimized in a $20\times20\times20$ $Å^3$ cubic cell, and the corresponding Brillouin-zone *k*-point mesh sampling was restricted to the gamma point. The electronic ground state was determined by the residual minimization method with an energy criterion of 0.01 meV, and geometries were relaxed using the conjugate gradient algorithm until ionic forces on each atom were less than 0.02 eV/Å. To search for more energetically favorable TM_{13} clusters by scanning larger structural configuration space, first-principles *NVT* velocity scaling molecular dynamics (MD) based on the SA (Ref. 42) method were performed. The whole simulation time was 10 ps and the time for each step was set to 10 fs.

Other systems with various dimensionalities and depicted in Fig. 2 were modeled: TM_4 clusters [Figs. 2(a) and 2(b), $15\times15\times15$ $Å^3$ cubic cell, Γ point], one-dimensional (1D) scales [Figs. 2(c) and 2(d)], double-scales [Figs. 2(e) and 2(f)], 1D-cylinders [Figs. 2(g) and 2(h)], 2D monatomic films and slabs [two and seven layers, fcc and simple cubic (sc) structures, 20 Å vacuum, and $15\times15\times1$ *k*-point mesh]. All the systems were fully relaxed (unconstrained atomic positions and cell size), except seven layer slabs for which only atomic positions were optimized.

Mulliken bond overlap population (BOP) (Ref. 43) was calculated with the CASTEP software[44,45] using the PW91 functional and a $20\times20\times20$ $Å^3$ cubic cell. Such an analysis only stands for structures exhibiting significant covalency so that it was restricted to TM_4.

III. RESULTS

A. New TM_{13} structures

To explore efficiently relevant conformations by the SA procedure, it is essential to choose an adequate annealing temperature for the TM_{13} clusters, depending on their binding energies (E_b). As expected, the stronger the binding energy of the metal, the higher the required SA maximal temperature. For example, we have found many amorphous and more stable isomers than NBP-Au_{13} by performing MD

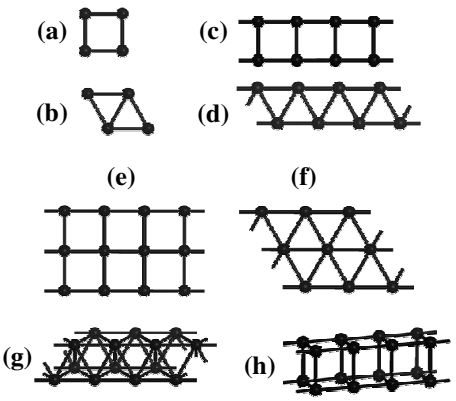

FIG. 2. (a) TM_4 square isomer; (b) TM_4 rhombus isomer. 1D-infinite periodic systems: [(c) and (d)] scales; [(e) and (f)] double scales; [(g) and (h)] cylinders.

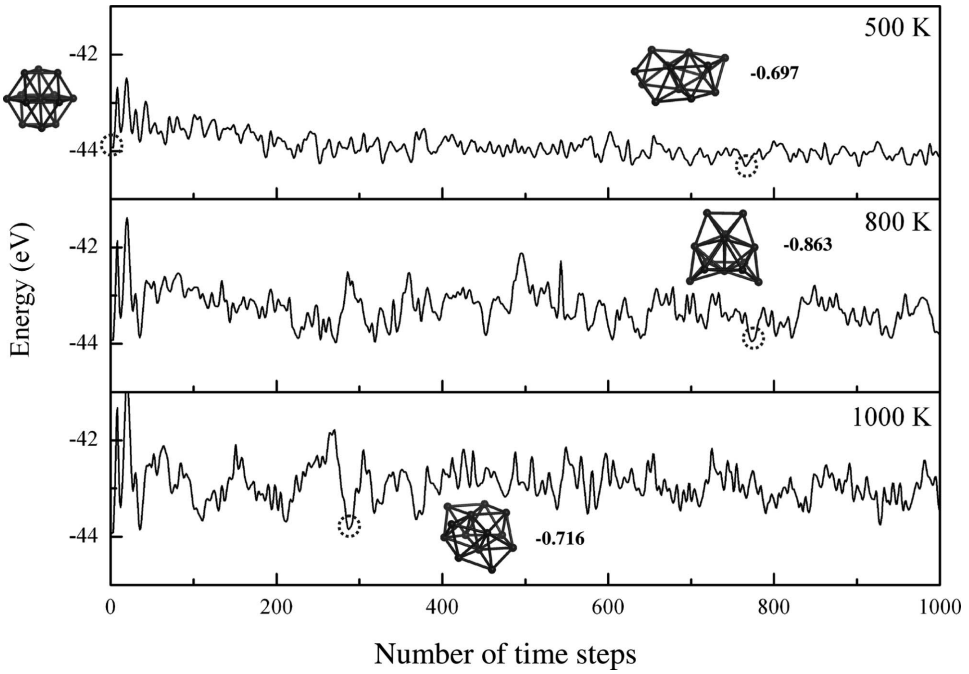

FIG. 3. Energy evolution versus the MD simulation steps at 500, 800, and 1000 K for Pd_{13} cluster with initial cuboctahedral (CUB) structure. The relaxed low-energy isomers, as well as their corresponding energy difference with respect to CUB-Pd_{13} are shown in insets.

simulations, starting from CUB-Au_{13}, at different annealing temperatures (300, 500, 800, and 1000 K). Higher annealing temperatures lead the atomic structure of Au_{13} to become much more planar and less stable: the most favorable isomer has been isolated with an annealing temperature of 300 K and is depicted on Fig. 1(i). However, for other TM_{13} with higher binding energies (Ru, Os, and Ir), annealing temperatures above 1000 K are necessary to find more energetically favorable structures. Palladium is an intermediate case for which the SA method provides an interesting structure for 800 K, as shown in Fig. 3.

According to our findings by SA-MD simulations and structures investigated by others (see introduction), 14 low-lying isomers are considered in the present work and presented in Fig. 1. The calculated results including the average nearest-neighbor distances d_{NN}, binding energies (E_b), and magnetic moments (M) for the most stable 4d and 5d TM_{13} clusters are summarized in Table I. Also reported in Table I are the ratio of square to triangular facets, $R_{s/t}$, and the parameter $\langle \rho_v \rangle = (d+s)/[4/3\pi(d_{NN}/2)^3]$, where d and s stand, respectively, for the numbers of d and s valence electrons in the electronic configuration of the element. $\langle \rho_v \rangle$ gives an estimation of the average density of valence electrons. Tables II and III provide additional data on relevant metastable TM_{13} structures useful for a systematic comparison of the structural stability. The coordinates of some relevant asymmetric clusters are reported in Sec. 1 of Ref. 46.

It can be first observed that TM_{13} clusters exhibit a great structural diversity. Contrary to the proposal of Ref. 17, the BBP isomer is not a universally stable structure for 13-atom late 4d TM_{13} clusters. We thus find more stable morphologies than BBP for all TM_{13} investigated here. For Tc, the SA-MD at 300 K reveals an energetically favorable structure [Fig. 1(j)], about 0.25 eV more stable than the NBP isomer [Fig. 1(d)]. For Re, varying the SA temperatures does not lead to more stable structures than the NBP isomer. For Rh and Ir, a SCSC structure [Fig. 1(g)] is the most stable, in agreement with the results of previous works.[21,26] For Ru_{13} and Os_{13}, a dSCSC isomer [Fig. 1(h)] is found as the most stable, consistently with the recent calculations by Li *et al.*[22] For Pt_{13}, two stable isomers Pt_SA [Fig. 1(k)] and Pt_SA2 [Fig. 1(l)] with similar E_b values (3.85 and 3.84 eV/atom) are

TABLE I. Calculated average nearest-neighbor distances d_{NN} (Å), binding energies E_b (eV/atom), magnetic moments M (μ_B/atom), $\langle \rho_V \rangle$ (see text) and ratio of square over triangular facets $R_{s/t}$ for the most stable TM_{13} clusters. The notation of the TM_{13} structures is given in Fig. 1.

	Structure (see Fig. 1)	d_{NN} (Å)	E_b (eV/atom)	M (μ_B/atom)	$\langle \rho_V \rangle$ (e^-/Å^3)	$R_{s/t}$
4d TM						
Tc	(j)	2.528	4.70	0.077	0.827	0.25
Ru	(h)	2.421	5.44	0.462	1.077	1.00
Rh	(g)	2.446	4.15	0.692	1.175	2.25
Pd	(d)	2.695	2.33	0.462	0.976	0.00
	(m)	2.713	2.33	0.615	0.917	
Ag	(n)	2.840	1.67	0.077	0.956	0.00
5d TM						
Re	(d)	2.550	5.15	0.308	0.806	0.00
Os	(h)	2.449	5.74	0.308	1.040	1.00
Ir	(g)	2.452	5.27	0.231	1.166	2.25
Pt	(k)	2.623	3.85	0.154	1.058	0.50
Au	(i)	2.807	2.10	0.077	0.950	0.00

TABLE II. Calculated average bond distances d (in Å), binding energies E_b (in eV/atom), and magnetic moments M (in μ_B/atom) for 4d energetically metastable TM_{13} clusters. NM means nonmagnetic.

	Structure (see Fig. 1)	d_{NN} (Å)	E_b (eV/atom)	M (μ_B/atom)
Tc	ICO	2.602	4.40	1.000
	CUB	2.514	4.46	0.154
	BBP	2.551, 2.53[a]	4.54	0.692, 0.69[a]
	NBP	2.520	4.68	NM
Ru	ICO	2.609, 2.59[b]	5.17, 4.16[b]	0.923, 1.00[b]
	CUB	2.573, 2.53[b]	5.20, 4.04[b]	0.154, 1.08[b]
	BBP	2.527, 2.53[a]	5.23	0.462, 0.46[a]
Rh	ICO	2.655, 2.65[b], 2.67[c]	4.03, 3.79[b], 3.75[c]	1.308, 1.30[b], 1.615[c]
	CUB	2.611, 2.63[b]	3.97, 3.75[b]	1.462, 1.50[b]
	BBP	2.617, 2.60[a]	4.03	1.308, 1.31[a]
Pd	ICO	2.749, 2.75[b], 2.75[c]	2.31, 2.30[b], 2.28[c]	0.615, 0.62[b], 0.615[c]
	NBP	2.582	4.07	0.923
	CUB	2.700, 2.70[b]	2.27, 2.24[b]	0.462, 0.46[b]
	BBP	2.693, 2.69[a]	2.32	0.308, 0.31[a]
	SCSC	2.574	2.22	0.077
Ag	ICO	2.887	1.57	0.385
	CUB	2.833	1.59	0.077
	BBP	2.844, 2.85[a]	1.63	NM, 0.08[a]

[a]Calculated values from Ref. 17.
[b]Calculated values from Ref. 20.
[c]Calculated values from Refs. 18 and 19.

discovered by SA-MD, which are significantly more favorable than the CBPT isomer [Fig. 1(f)] proposed recently.[21] For Pd_{13}, an isoenergetic structure of NBP isomer is found [Fig. 1(m)]. For Ag_{13} and Au_{13}, amorphous structures [Figs. 1(n) and 1(i)] are more stable than the NBP isomer. This result illustrates the propensity of Ag and Au to give rise to

TABLE III. Calculated average bond distances d (in Å), binding energies E_b (in eV/atom), and magnetic moments M (in μ_B/atom) for 5d energetically metastable TM_{13} clusters. NM means nonmagnetic.

	Structure (see Fig. 1)	d_{NN} (Å)	E_b (eV/atom)	M (μ_B/atom)
Re	ICO	2.617	4.69	1.00
	CUB	2.547	4.85	0.462
	BBP	2.612	5.04	0.154
Os	ICO	2.590	5.23	0.154
	CUB	2.542	5.18	0.615
	BBP	2.543	5.51	0.308
Ir	ICO	2.637, 2.65[a]	4.78, 4.79[a]	0.154, 0.54[a]
	CUB	2.614, 2.61[a]	4.73, 4.74[a]	1.462, 1.46[a]
	BBP	2.636	5.00	0.242
Pt	ICO	2.728, 2.72[a], 2.73[b]	3.59, 3.58[a], 3.24[b]	0.154, 0.15[a], 0.154[b]
	CUB	2.694, 2.69[a]	3.61, 3.60[a]	0.462, 0.46[a]
	BBP	2.705	3.73	0.308 (0.462)
	NBP	2.683, 2.65[a]	3.75, 3.40[a]	NM, NM[a]
	PT_SA2	2.651	3.84	0.154
Au	ICO	2.887	1.88	NM
	CUB	2.837	1.99	NM
	BBP	2.886	2.05	NM

[a]Calculated values from Refs. 18 and 19.
[b]Calculated values from Ref. 17.

ductile structures[31,47] even if the exhaustive structural investigation of Au clusters is still a matter of research and beyond the scope of the present work due to the overestimation of *s-d* hybridization by DFT in favor of planarlike structures and to the influence of relativistic effects.[47–54]

B. Magnetic properties of TM_{13}

The occurrence of magnetism is a peculiar property of small TM clusters accompanied by the reduction in coordination number (CN) and localization of electrons compared to the bulk materials. Nonmagnetic materials can thus give rise to magnetic clusters.[55,56] A high symmetry may lead to a highly degenerate highest occupied molecular orbital and favor high spin states.[8] On the contrary, the degeneracy is lifted and the ground state may prefer a lower spin state when the symmetry is lowered. Our calculations recover that trend: most high-symmetry CUB and ICO isomers indeed exhibit higher magnetic moment (M) than others with lower symmetry (see Tables I–III).

The calculated M for ICO-Ru_{13} and ICO-Rh_{13} are 0.923 and 1.615μ_B/atom, which are consistent with other theoretical calculations,[12,13,17,18,20,22,32] however, too high compared to experimental values (Ru_{13}: maximal value 0.29μ_B/atom; Rh_{13}:0.48μ_B/atom).[56] The new dSCSC-Ru_{13} (0.462μ_B/atom) and SCSC-Rh_{13} (0.692μ_B/atom, consistent with Ref. 26) clusters significantly reduce the discrepancy between experiments and theory. Thus, the cluster shape greatly influences its magnetic properties. In addition, due to the high local magnetic moments of corner atoms, the calculated M of the lowest-energy Pd_{13} [Figs. 1(d) and 1(m), NBP and Pd_SA, respectively) reaches 0.462μ_B/atom and 0.615μ_B/atom and is also enhanced in spite of their rather low symmetry (C_{3v} and C_{2v}, respectively). The value for NBP-Pd_{13} is consistent with earlier calculations[18] and with the upper experimental limit reported by Cox *et al.*[56] (0.40μ_B/atom), whereas the values for Pd_SA and ICO-Pd_{13} (0.615μ_B/atom, in agreement with previous works[6,14,15,18,23,57]) are still too high. For Pt_{13}, the calculated M (0.154μ_B/atom) is much lower than the recent experimental value[8] (0.655μ_B/atom) even if improved compared to the extensively studied nonmagnetic NBP-Pt_{13}. This discrepancy can be largely due to the fact that the value reported in Ref. 8 stands for $Pt_{13\pm2}$ in a zeolite: the support can be at the origin of significant variation in the magnetic properties. For Ag_{13} and Au_{13}, the lower M value close to zero in their low-lying isomers is explained by considering their fully occupied d shell. In addition, we find that the calculated M of the lowest-energy 4d TM isomers is generally higher than that of 5d TM isomers when considering the isomers with similar valence electron configuration, resulting from the larger delocalization of 5d states.

C. Comparison with model systems of increasing dimensionality

In these competing structures, two kinds of surface building units mainly exist: the square planar facet [fcc or sc (100) type] and the triangular planar facet [fcc (111) type]. The number of square and triangular facets (hereafter, n_s and n_t) in each cluster's conformation is different. For example, SCSC [Fig. 1(g)] and TCSC [Fig. 1(e)] include as many square facets as possible, whereas for isomers in Figs. 1(a), 1(b), 1(d), 1(i), 1(m), and 1(n), for example, the triangular facets are predominant. The nonmonotonic variations in the ratio of the square to triangular facets ($R_{s/t}=n_s/n_t$) and of the CN of the most stable isomers versus TM elements are plotted in Fig. 4. It clearly shows that for the late 4d and 5d TM elements with similar electron configuration, the TM_{13} clusters (in the lowest-energy isomers) exhibit similar $R_{s/t}$ value. $R_{s/t}$ reaches a maximum value (9/4) in the case of the SCSC isomer (Rh_{13} and Ir_{13}). In addition, Table I shows that $R_{s/t}$ is correlated with the parameter $\langle \rho_v \rangle$, indicating that valence electrons tend to become more confined for systems with more square facets.

To propose a rationale for this structural trend, we further investigate the relative stability of optimized systems with various dimensionalities exposing either only triangular or square facets: TM_4 clusters [Figs. 2(a) and 2(b)], 1D scales [Figs. 2(c) and 2(d)], double scales [Figs. 2(e) and 2(f)], 1D cylinders [Figs. 2(g) and 2(h)], 2D monatomic films and slabs (two and seven layers, fcc and sc structures). Even if TM_4 tetrahedron is also known to be favored for some metals, the two planar isomers have been chosen as reference systems.

The binding energies of the most stable geometry (square or triangle facetted) for each element and each kind of system is reported in Fig. 5. It first shows that E_b goes through a maximum, for 4d (Ru) and 5d (Os) metals independently, whatever the system. The absolute variations in E_b for TM_{13} clusters are thus primarily an effect of the nature of the metallic element, which can be related to the d band filling. As expected, E_b increases monotonically from TM_4 to the bulk, together with the metal CN and the dimensionality. Nevertheless, the most stable geometry (triangle or square faceting) for a given metal is dimensionality dependant. Three classes of systems can be distinguished from the following analysis:

(i) Systems exhibiting triangular facets whatever the element under study, mainly, the systems with the larger dimensionality such as two and seven layers slabs, and also monoatomic film of 5d metals.

(ii) Systems exhibiting square facets for the lowest d electrons numbers (Tc, Ru, Rh, and eventually Pd; Re, Os, Ir, and eventually Pt) and triangular facets for the highest (Ag, eventually Pd; Au, eventually Pt): mainly, the scales, double scales for 4d metals, and TM_4 clusters.

(iii) Systems exposing square facets for intermediate number of electrons (Ru and Rh, Os and Ir): namely, cylinders, double scales for 5d metals, and TM_{13} clusters (Fig. 4).

For model palladium systems exhibiting triangular or square facets as well as for the fcc bulk, NBP (triangular facets, most stable Pd_{13} cluster), and SCSC (mainly square facets) TM_{13}, we first analyze valence DOS normalized per atom. The results are depicted in Fig. 6(A). The analogous results for the two relevant Rh-NBP and Rh-SCSC TM_{13}, and Tc_SA and Tc-TCSC systems are reported in Figs. 6(B) and 6(C), respectively. The first and second moments I_n [n =1 and 2 in Eq. (1)], as defined in Ref. 57, are evaluated to quantify the valence states below the Fermi level (ε_f);

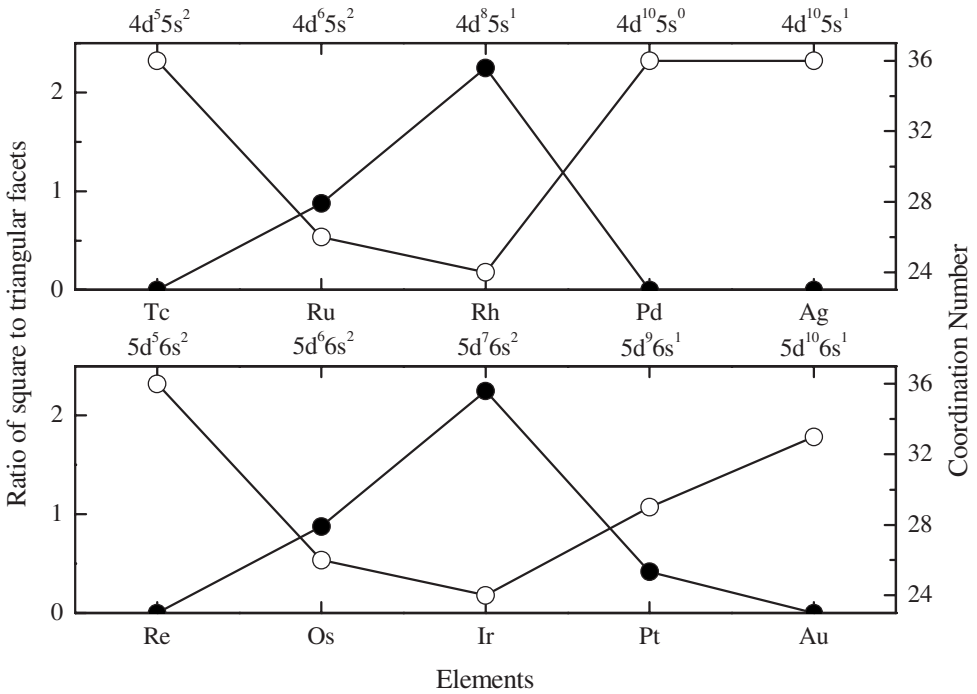

FIG. 4. Ratio of square to triangular facets (solid circle) and coordination number (hollow circle) for the most stable 13-atom late 4*d* and 5*d* TM clusters. The atomic valence electron configuration for TM elements is given at the top of each panel.

$$I_n = \int_{-\infty}^{\varepsilon_f} N(\varepsilon)\varepsilon^n d\varepsilon \tag{1}$$

I_0 stands for the total number of occupied states of the system. The ratio I_1/I_0 represents the center of gravity of the occupied valence states of the DOS, whereas the ratio I_2/I_0 (with the energy ε referred to the center of gravity of the DOS) is proportional to the mean square width of the occupied states. The numerical values of I_1 and I_2 are reported in Table V of Sec. 2 in Ref. 46. It can be first noticed that the center of the DOS (I_1/I_0) increases as the dimensionality of the system decreases, from bulk to TM_4 clusters, and simultaneously the states become more discrete due to the reduced number of coordination when the dimensionality becomes smaller. In contrast, the width of the DOS (I_2/I_0), decreases as the dimensionality of the system decreases. The evolutions of I_1 and I_2 are thus qualitatively interdependent, and a qualitative correlation between the binding energy E_b, I_1/I_0 and I_2/I_0 can moreover be drawn in Figs. 7(a) and 7(b) throughout the series. In the case of the seven layers slab [sc (100) and fcc (111) surfaces], we obviously recover results in line with the *d*-band model:[58] the more compact periodic system [such as the fcc (111) surface] shifts down its value of I_1/I_0 and expands the width of its occupied band (I_2/I_0) with respect to systems with less confined electronic density [such as the sc (100) surface]. However, for a Pd system with a lower dimensionality (smaller than two layers slab), the preferred morphology is not anymore reflected by the values of I_1/I_0. See, for example, the double scales (triangular: $I_1/I_0=-1.69$ eV and $E_b=2.25$ eV/atom; square: $I_1/I_0=-1.80$ eV and $E_b=2.12$ eV/atom) or TM_{13} (Pd-NBP: $I_1/I_0=-1.78$ eV and $E_b=2.33$ eV/atom; Pd-SCSC: $I_1/I_0=-1.94$ eV and $E_b=2.22$ eV/atom). This result suggests that some specific electronic effects involved in small dimensionality systems (with very low coordinated atoms) cannot be captured by the average position of the occupied valence state. Among these effects, it can be invoked the covalent character of the metal-metal bond, the Pauli repulsion and the Coulombic repulsion between bonding basins, which influence the shape and the width of the occupied states independently from the center of gravity of these states. These effects become predominant for the determination of the structure, as it will be discussed in Sec. IV. The DOSs of SCSC-Rh_{13} (the most stable Rh_{13} cluster) and NBP-Rh_{13} are also shown in Fig. 6(B). In that case, the respective values of I_1/I_0 are again not representative of the relative stabilities of the isomers (Rh-NBP: $I_1/I_0=-2.53$ eV and $E_b=4.07$ eV/atom; Rh-SCSC: $I_1/I_0=-2.47$ eV and $E_b=4.15$ eV/atom).

If one considers the values taken by I_2/I_0, Figs. 6(A) and 7(b)) first reveal that the width of the valence band clearly depends on the dimensionality of the Pd systems. The smaller the system's size is, the weaker the electronic delocalization is and the stronger the contraction of the occupied band. Furthermore, when comparing the Pd and Rh TM_{13} systems, it appears that the width of the band is larger for Rh than for Pd. Indeed, the *d*-band width of bulk 4*d* fcc metals decreases from Tc to Ag, which can be related to the increase in the effective screened nuclear charge from left to right in a period and thus to more contracted orbitals, as suggested by the Slater's rule. According to the I_2/I_0 values obtained for the most stable Tc_{13} (2.25 eV^2 for TC_SA), Rh_{13} (2.01 eV^2 for SCSC), and Pd_{13} (1.44 eV^2 for NBP) as reported in Table V of Sec. 2 of Ref. 46, this trend remains thus valid for TM_{13} clusters, meaning that the I_2/I_0 value seems to be an interesting parameter.

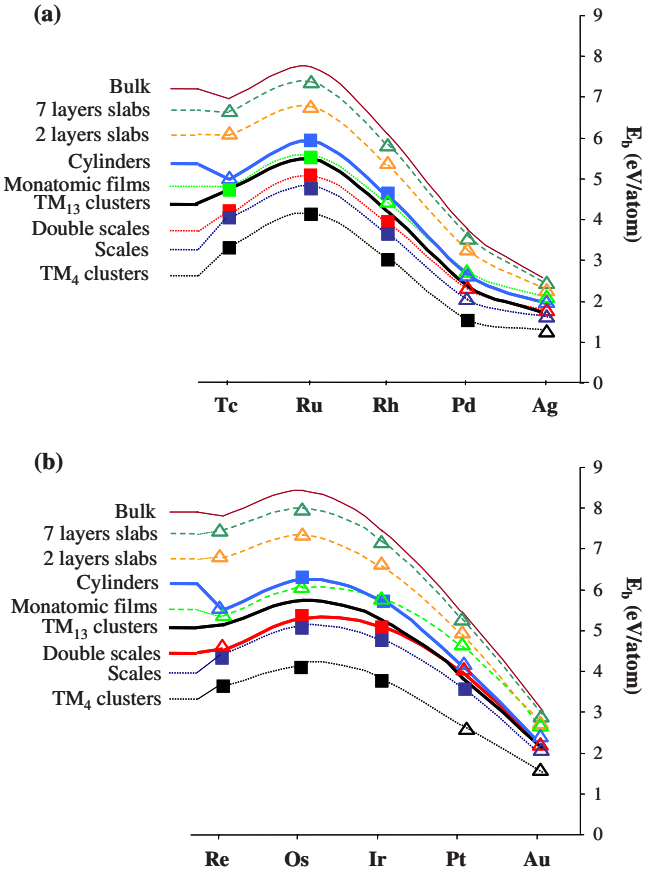

FIG. 5. (Color online) Calculated binding energies (E_b) for 4d (a) and 5d (b) metallic systems of Figs. 1 and 2, corresponding to the most stable facets. Squares (■) and triangles (△) correspond to most stable systems, among square and triangle facets, respectively. Dotted lines (……) correspond to systems exposing square facets for the low d electrons numbers, and triangle for the higher. Bold lines (−) correspond to systems exposing square facets at intermediate number of electrons. Dashed lines (---) indicate systems always exposing triangle facets.

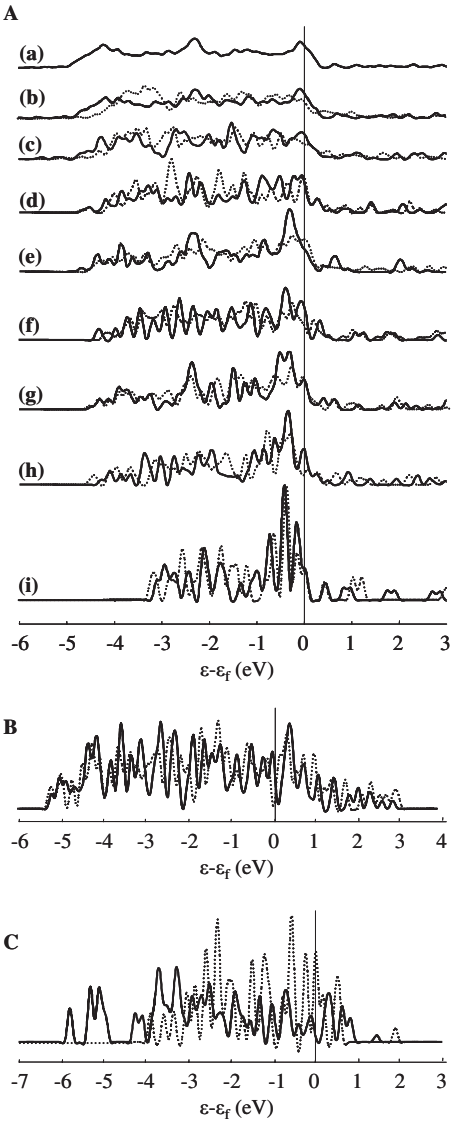

FIG. 6. Density of states (DOS) for square (dotted lines) and triangle (full lines). A: For palladium, (a) fcc bulk; (b) seven layers slabs, fcc (111) (full line), sc (100) (dotted line); (c) two layers slabs; (d) cylinders; (e) monatomic films; (f) TM_{13} NBP (full line) and SCSC (dotted line); (g) double scales; (h) scales; (i) TM_4 planar clusters, rhombus (full line) and square (dotted line). B: Rh-TM_{13}, NBP (full line) and SCSC (dotted line). C: Tc-TM_{13}, Tc_SA(full line) and TCSC (dotted line).

Figure 7(c), which depicts triangle minus square binding energies as a function of I_2/I_0 differences, illustrates that point. However, it also reveals that for square versus triangle isomers of Pd_4 and Rh_{13} clusters, the relative stability is not given by the ordering of their I_2/I_0 values. The bandwidth difference between the NBP and SCSC TM_{13} isomer for Rh is moreover tiny (close to the value found for the Pd_4 system). The accuracy of I_2/I_0 in describing the relative stability of isomers will be discussed in the forthcoming section.

IV. DISCUSSION

A. Square vs triangle

Using simulated annealing methods with carefully adjusted annealing temperature, we have been able to discover new morphologies for 13-atom clusters of late transition metals. Some of them are in better agreement with experiments for what concerns magnetic properties than previously reported structures. In what follows, we provide elements for the interpretation of the structural diversity by shedding light on periodic trends between electronic and geometric feature. Figure 4 shows that the morphology of TM_{13} clusters does not follow a monotonic behavior since the ratio of square to triangular facets $R_{s/t}$ reaches a maximum for TM=Rh and Ir. Even if some more stable structures might be found in the future, we are quite confident with this trend as the strong affinity of Ru, Rh, and Ir clusters for square facets have also been reported in recent published works.[20–22,26,27,29,32]

Intrinsically, square facets correspond to lower bond lengths, as observed for all the systems simulated within this work. This trend can be seen as a consequence of the fact that the lobes of d orbitals are at 90° of each others so that d-type bonding should *a priori* favor 90° bond angles, as

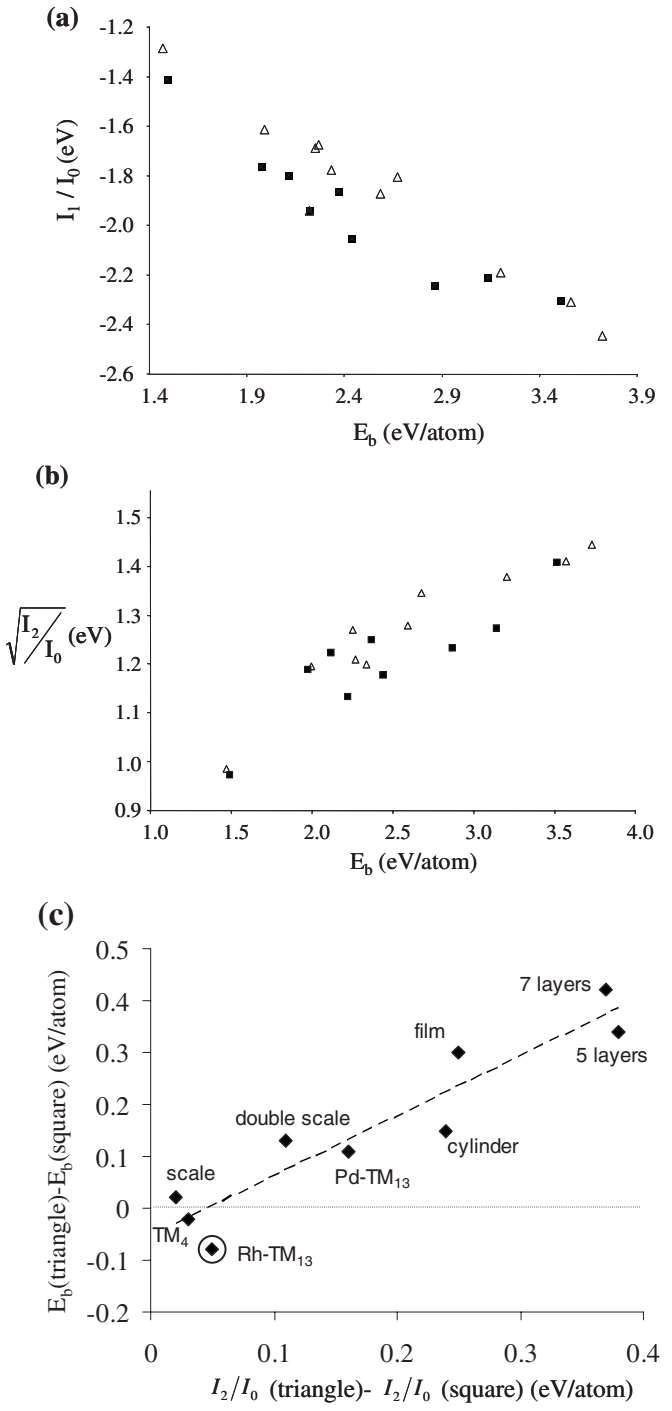

FIG. 7. Correlations between the binding energy and (a) the ratio I_1/I_0, (b) the value of $\sqrt{I_2/I_0}$, for Palladium systems of various dimensionality, exhibiting square (full squares) and triangular facets (empty triangles), (c) the difference in binding energies between the systems exhibiting triangular and square facets as a function of their I_2/I_0 differences (including Rh-TM_{13}).

proposed by Sun *et al.*[29] However the existence of square facets is related to lower coordination numbers than that of triangular facets, as illustrated in the case of TM_{13} in Fig. 4. Triangular facets thus induce higher number of bonds per atom, separated by a lower angle (~60°) than squares (~90°). By maximizing the orbital overlap and at the same time limiting repulsions, the relative binding energy of isomers for a given metal indeed results from several antagonist factors:

TABLE IV. Bond overlap population (BOP) of 4*d* and 5*d* TM_4 for the square or rhombus isomer

	Square		Rhombus	
4*d* TM	Total	Per bond	Total	Per bond
Tc	3	0.75	2.88	0.58
Ru	2.6	0.65	2.26	0.45
Rh	2.12	0.53	2.01	0.40
Pd	1.2	0.30	1.47	0.29
Ag	1.56	0.39	1.76	0.35
5*d* TM				
Re	3.8	0.95	3.8	0.76
Os	3.52	0.88	2.93	0.59
Ir	3.12	0.78	2.76	0.55
Pt	1.88	0.47	2	0.40
Au	1.48	0.37	1.56	0.31

(i) Effect (1): the maximum number of bonds, in favor of maximum coordination number, e.g., triangular facets.

(ii) Effect (2): the minimum bond length (e.g., high covalence degree, with maximal overlap), in favor of squares. On the lower range of dimensionality, such as TM_4 clusters, the contraction of the bandwidth is maximal and the DOS shape reveals a different nature of states which are becoming more discrete [Fig. 6Ai]. The calculated Mulliken BOPs per bond, reported in Table IV, indicates indeed the covalent character of the bond. Furthermore, the value is always higher for a bond belonging to a square than for a bond relative to a rhombus, whatever the metal and the preferred geometry of the TM_4 cluster. The BOP decreases along the 4*d* and 5*d* rows, showing evidence for less and less covalent bonds.

(iii) Effect (3): Pauli repulsion. Qualitatively, this last effect should increase as the number of electrons per bond increases. For a given number of atoms, electrons are shared between more numerous bonds for triangles facets (for example, in the case of TM_4, electrons are shared between four bonds for the triangle vs five bonds for the rhombus) that is to say that Pauli repulsion is lower for the rhombus than for the square.

(iv) Effect (4): Coulombic repulsion between bonds. For squares and triangles of same edge length a, the distances between edge centers are longer by $\sqrt{2}$ for squares; but as shown for effect (3), there are fewer electrons per bonds in the case of the rhombus. Numbering all repulsion terms between the centers of all bonds (see details in Sec. 3 of Ref. 46), the total Coulombic term q^2/r is thus $0.48N^2/a$ for the square and $0.65N^2/a$ for the rhombus, where N is the number of electrons of the TM_4 cluster and a is the supposed common edge length of the square and the rhombus. As explained in Sec. 3 of Ref. 46, this trend can also be generalized to larger dimensionality system. The Coulombic repulsion is thus by nature lower for the square. The fact that

chemical bonds belonging to square facets are shorter than bonds belonging to triangular facets [effect (2)] can counterbalance this conclusion in favor of squares.

In what follows, we try to infer which of these effects is predominant, depending on the dimensionality of the system and on the nature of the metal, so as to understand the trends observed.

B. Impact of dimensionality

The gradual transition of clusters facets from square to triangles as the size of the aggregate increases is documented for several late transition metals.[26,27,32,57] Here we show that such a feature can be generalized to model systems of increasing dimensionality, from TM_4 clusters to extended slabs, but that the level of dimensionality at which this transition occurs is metal dependant. TM_{13} exhibit an intermediate E_b close to double scales and cylinders (Fig. 5). We were moreover able to capture a similar behavior for cylinder ($4d$ and $5d$) and double scale ($5d$ only) systems, with a preferred square symmetry for Ru, Rh, Os, and Ir. Systems with lower dimensionality exhibit only a single square to triangle transition along the row (within late $4d$ and $5d$ TM), whereas more extended systems are always triangular. This means that the maximum reported in Fig. 4 is a feature that can be generalized to intermediate dimensionality such as cylinders ($4d$ and $5d$), double scales ($5d$ only), and TM_{13} clusters.

For a given metal, increasing the dimensionality of the system induces gradual increase in the coordination number of atoms, in favor of effect (1). Meanwhile, the total overlap between orbitals for square geometries is not proportionally increased as a same orbital has to share overlaps with several neighbors: effect (2) increases but this growth is dominated by that of effect (1).

The dependency of effect (3) (Pauli repulsion) with dimensionality can be quantified by reasoning on a growing scale, starting from the rhombus (triangular scale) or a square (square scale). For a given number of atoms N_A in the growing scale, the number of bonds is $2N_A-3$ for the triangular scale and $3/2N_A-2$ for the square scale (see Sec. 4 of Ref. 46 for more explanation) so that each time two atoms are added along the scale, four and three additional bonds appear for the triangular and square scales, respectively. As the Pauli repulsion decreases with the increase in the number of bonds for a given number of atoms, it can be deduced that effect (3) favors triangles even more when the dimensionality increases.

Regarding effect (4), according to Sec. 3 of Ref. 46, the relative contribution of Coulombic repulsions between the rhombus and square configurations is given by the ratio $0.65/0.48 \sim 1.36$ in favor of the square for TM_4. This trend remains valid for TM_{13} and for systems with larger dimensionality (such as described in Sec. 3 of Ref. 46) where the relative contribution becomes smaller (ratio of about 1.13–1.20) but always in favor of the systems exhibiting squares.

The trend to convert into triangular structures as the dimensionality increases, observed for each metal (Fig. 5), thus appears as the consequences of effects (1) and (3), which dominate effects (2) and (4), more and more as the dimensionality increases. In Fig. 6(A), this is illustrated in the case of Pd by the observation of the rapid decrease in energy of the lowest states for triangular systems as the dimensionality increases, much more rapid than that of square systems: for TM_4 clusters, the square isomer exhibits the lowest-energy states, whereas square and triangular are competitive in the lowest-energy part of the DOS for double scales, and finally fcc (111) facets of seven layers slabs exhibit much more states at lower energy than sc (100) facets, for example.

As proposed in the previous section, this trend is recovered by the second moment of the DOS (I_2/I_0), quantifying the DOS bandwidth, which is likely related to effects (1), (2), and part of effect (3). In the case of Pd with dimensionality strictly larger than the 1D-scale, Fig. 7(c) illustrates that the value of the difference of the bandwidth between systems exhibiting square and triangular facets captures their relative stability. Indeed, the larger the width, the more stable the system which maximizes the number of metal-metal bonds. A further consequence of this broadening, which is much more pronounced for triangles, is that states appear as much more delocalized in the case of triangles for high dimensionality systems, providing minimization of the Pauli repulsion. Such a trend is much more pronounced for $5d$ metals, for which triangular monatomic films are universally preferred (see Fig. 5), due to more diffuse orbitals.

However, in the case of very small systems such as Pd_4 or Pd 1D scale, the values of I_2/I_0 are very small (due to band contraction resulting from low coordination numbers among others) and furthermore, the difference in the values of I_2/I_0 is close to 0 for the Pd_4 or Pd 1D-scale structures exhibiting either squares or triangular facets [Fig. 7(c)]. This result is also consistent with the similar values of BOP per bond found for Pd_4 rhombus and squares (Table IV). In addition, effect (4) (which is not reflected in the I_2/I_0 values), resulting from Coulombic repulsion between bonding basins, becomes predominant due to strongly localized electrons in those basins in low dimensionality structures. This implies that for very low dimensionality Pd systems such as TM_4 or 1D scale, the Coulombic repulsion (effect 4) may explain why the square facets compete with triangles. Moreover, the analysis reported in Sec. III C illustrates how the I_1/I_0 value (i.e., band center) is not strictly correlated with the I_2/I_0 values. Indeed, for a given dimensionality (such as cylinder, $TM_{13...}$), the I_2/I_0 is larger for the more stable structure, corresponding to a more expanded band width, allowing a minimization of the Pauli repulsion, which is not always reflected by I_1/I_0.

In what follows, we attempt to extrapolate this analysis to other metallic elements exhibiting close bandwidths.

C. Impact of the nature of the metal

From one metal to another in the same row, effects (1)–(4) are weighted differently, resulting in various sensitivity to the increase in dimensionality, starting from TM_4. For nearly filled d-band metals (Pd and Ag; Pt and Au), effect (2) becomes negligible insofar as antibonding d states are nearly filled. This already comes out from the BOP analysis for TM_4 clusters (Table IV), reaching the lowest values of all

metals studied. Effect (2) is thus dominated by effects (1), (3), and (4). The evolution of effects (3) (Pauli repulsion) and (4) (Coulombic repulsion) as the number of electrons increases is roughly the same for square and triangular facets, thus inducing almost no change in the morphology orientation. Effect (1) thus remains to explain that the late *d* metals strongly prefer triangular facets.

Other metals with open *d* band and for which more electrons are involved in bonding than antibonding filled shells are far more sensitive to effect (2), which explains their higher affinity for square facets than the latest *d* metals, in the limit of the high dimensionality as shown in Sec. IV B. In particular, this trend is stronger for Ru (Os) and Rh (Ir) than for Tc (Re), whereas a simple reasoning on *d*-band filling would have favored Tc (Re) due to the maximal bonding states occupied (d^5).

The contraction of the DOS as suggested by Slater has again two antagonist effects: increase of covalency [effect (2), in favor of square] together with an increase in the Pauli repulsion [effect (3), in favor of triangles], the latter dominating for the nearly *d*-filled band due to more numerous electrons. We thus agree with Sun *et al.*[29] that this can provide interpretation for the maximum at d^6 or d^7 instead of d^5.

The energetic manifestation of these antagonist effects is that the maximum in binding energy for all systems (Fig. 5) is not centered on Tc and Re but rather on Ru and Os. From a structural aspect ($R_{s/t}$ value), the present work demonstrates that the $R_{s/t}$ maximum is also shifted from d^5 to d^7 but only for systems of intermediate dimensionality as TM_{13} (Fig. 4). More extended systems are indeed dominated by effects (1) and (3) (favoring triangle) and less extended systems by effects (2) and (4) (where square usually prevail), as discussed in the preceding section. This reinforces the interest for metallic systems in this dimensionality range: some periodic effects are observed for extended systems, due to variations in electronic properties,[58] and it can be expected that for intermediate dimensionality systems these electronic effects will be combined to a geometric one (itself a consequence of electronic effects), consisting in a variable $R_{s/t}$.

In Sec. IV B, the I_2/I_0 was shown to be an appropriate tool to monitor the effect of dimensionality in the case of Pd systems, except for the smallest systems Pd_4 and Pd-1D scales. We now consider the additional cases of Rh and Tc. Figure 7(c) reveals that the bandwidth difference between the NBP and SCSC TM_{13} isomer for Rh is close to zero. Even if the bandwidth is much larger than for Pd_{13}, effects (1)–(3), as well as the I_2/I_0 value are not determining (as in the case of Pd_4 and Pd-1D scale, see Secs. III C and IV B). On the contrary, the value found for the Coulombic repulsion between bonding basins in the case of the two Rh_{13} isomers show that effect (4) is in favor of the square facets (the Coulombic repulsion ratio is close to 1.16 as described in Sec. 3 of Ref. 46). The fact that the bandwidths (I_2/I_0 values) of the two Rh_{13} isomers are nearly identical implies that the minimization of the Coulombic repulsion (not given by the I_2/I_0 value) explains the high $R_{s/t}$ value observed for this metal. Decreasing even more the dimensionality of the Rh systems (such as double scales, scales or TM_4) keeps stabilizing the square facets, as a result of the predominant effect (4). If we now consider the case of Tc_{13}, which exhibits a low $R_{s/t}$ value as found for Pd systems, the difference of the bandwidth between the most stable Tc_SA structure and the TCSC structure maximizing the number of square facets, is clearly in favor of the Tc_SA structure (see Table V of Sec. 2 of Ref. 46). A similar I_2/I_0 value is obtained for the NBP structure (also maximizing triangular facets as Tc_SA), which indicates that, in the case of Tc, the second moment of the occupied band must be regarded as the electronic descriptor of the most stable structure maximizing the number of triangular facets (as in the case of Pd systems with large dimensionality).

V. CONCLUSIONS

This work has proposed a systematic investigation of the structural, energetic and electronic properties of late 4*d* and 5*d* transition-metal systems (from Tc to Ag, and from Re to Au). This investigation has also included the determination of TM_{13} structures by simulated annealing DFT molecular dynamics. New energetically stable TM_{13} structures not being reported previously have been discovered, some of them exhibiting closer magnetic properties as compared to experiments than previously reported structures. Their structural diversity can be rationalized thanks to the variation in the $R_{s/t}$ ratio of square to triangular facets as a function of the periodic filling of valence electrons. $R_{s/t}$ reaches its maximum for Rh_{13} and Ir_{13}, which is shown to be typical of intermediate-dimensionality systems, as 1D cylinders and double 1D scales. The observed variations of the ratio $R_{s/t}$ with *d*-band filling and dimensionality result from four competing effects: coordination numbers, covalent bonding character, the Pauli and Coulombic repulsions. The DOS analysis and the systematic calculations of the first and second moments of the occupied valence states have shown that the stability of systems exposing triangular facets corresponds to a maximal value of the second moment (i.e., bandwidth), which is regarded as a maximization of the coordination number and a minimization of Pauli repulsion. In contrast, systems exposing mainly square facets (such as Rh_{13}, and other low dimensionality systems) maximize the covalent character of the bonding and minimize the Coulombic repulsions between the bonding basins.

The original behavior of TM_{13} clusters and intermediate dimensionality systems exposing more square facets for Ru (Os) and Rh (Ir) might show a pathway for designing materials with improved physical (e.g., magnetic) properties as well as chemical (e.g., catalytic) properties.

ACKNOWLEDGMENTS

This work has been performed within the SIRE project (Grant No. ANR-06-CIS6-014-04) sponsored by the Agence Nationale de la Recherche (ANR).

*Present address: Department of Information Materials Science and Engineering, Guilin University of Electronic Technology, Guangxi 541004, People's Republic of China.
†pascal.raybaud@ifp.fr

[1] M. Haruta, Catal. Today **36**, 153 (1997).
[2] H.-J. Freund, Surf. Sci. **500**, 271 (2002).
[3] J. Bansmann, S. H. Baker, C. Binns, J. A. Blackman, J.-P. Bucher, J. Dorantes-Dávila, V. Dupuis, L. Favre, D. Kechrakos, A. Kleibert, K.-H. Meiwes-Broer, G. M. Pastor, A. Pérez, O. Toulemonde, K. N. Trohidou, J. Tuaillon, and Y. Xie, Surf. Sci. Rep. **56**, 189 (2005).
[4] W. L. Barnes, A. Dereux, and T. W. Ebbesen, Nature (London) **424**, 824 (2003).
[5] Y. P. Chiu, L. W. Huang, C. M. Wei, C. S. Chang, and T. T. Tsong, Phys. Rev. Lett. **97**, 165504 (2006).
[6] N. Watari and S. Ohnishi, Phys. Rev. B **58**, 1665 (1998).
[7] U. Kreibig and M. Vollmer, *Optical Properties of Metal Clusters* (Springer, New York, 1995).
[8] X. Liu, M. Bauer, H. Bertagnolli, E. Roduner, J. van Slageren, and F. Phillipp, Phys. Rev. Lett. **97**, 253401 (2006).
[9] E. Bus, D. E. Ramaker, and J. A. van Bokhoven, J. Am. Chem. Soc. **129**, 8094 (2007).
[10] E. Bus and J. A. van Bokhoven, Phys. Chem. Chem. Phys. **9**, 2894 (2007).
[11] M. Calleja, C. Rey, M. M. G. Alemany, L. J. Gallego, P. Ordejón, D. Sánchez-Portal, E. Artacho, and J. M. Soler, Phys. Rev. B **60**, 2020 (1999).
[12] B. V. Reddy, S. K. Nayak, S. N. Khanna, B. K. Rao, and P. Jena, Phys. Rev. B **59**, 5214 (1999).
[13] L. Wang and Q. Ge, Chem. Phys. Lett. **366**, 368 (2002).
[14] M. Moseler, H. Häkkinen, R. N. Barnett, and U. Landman, Phys. Rev. Lett. **86**, 2545 (2001).
[15] V. Kumar and Y. Kawazoe, Phys. Rev. B **66**, 144413 (2002).
[16] O. D. Häberlen, S.-C. Chung, M. Stener, and N. Rösch, J. Chem. Phys. **106**, 5189 (1997).
[17] C. M. Chang and M. Y. Chou, Phys. Rev. Lett. **93**, 133401 (2004).
[18] T. Futschek, M. Marsman, and J. Hafner, J. Phys.: Condens. Matter **17**, 5927 (2005).
[19] T. Futschek, J. Hafner, and M. Marsman, J. Phys.: Condens. Matter **18**, 9703 (2006).
[20] W. Q. Zhang, L. Xiao, Y. Hirata, T. Pawluk, and L. C. Wang, Chem. Phys. Lett. **383**, 67 (2004).
[21] L. L. Wang and D. D. Johnson, Phys. Rev. B **75**, 235405 (2007).
[22] S. F. Li, H. S. Li, J. Liu, X. L. Xue, Y. T. Tian, H. He, and Y. Jia, Phys. Rev. B **76**, 045410 (2007).
[23] C. Luo, C. Zhou, J. Wu, T. J. Dhilip Kumar, N. Balakrishnan, R. C. Forrey, and H. Cheng, Int. J. Quantum Chem. **107**, 1632 (2007).
[24] R. C. Longo and L. J. Gallego, Phys. Rev. B **74**, 193409 (2006).
[25] Y. C. Bae, H. Osanai, V. Kumar, and Y. Kawazoe, Phys. Rev. B **70**, 195413 (2004).
[26] Y. C. Bae, V. Kumar, H. Osanai, and Y. Kawazoe, Phys. Rev. B **72**, 125427 (2005).
[27] T. Pawluk, Y. Hirata, and L. Wang, J. Phys. Chem. B **109**, 20817 (2005).
[28] L. Xiao and L. Wang, J. Phys. Chem. A **108**, 8605 (2004).
[29] Y. Y. Sun, M. Zhang, and R. Fournier, Phys. Rev. B **77**, 075435 (2008).
[30] J. Rogan, G. Garcia, C. Loyola, R. Ramírez, and M. Kiwi, J. Chem. Phys. **125**, 214708 (2006).
[31] J. Oviedo and R. E. Plamer, J. Chem. Phys. **117**, 9548 (2002).
[32] G. Zhang, H. Zhao, and L. Wang, J. Phys. Chem. B **108**, 2140 (2004).
[33] F. H. Stillinger and T. A. Weber, J. Chem. Phys. **80**, 4434 (1984).
[34] J. Cheng and R. Fournier, Theor. Chem. Acc. **112**, 7 (2004).
[35] G. Kresse and J. Hafner, Phys. Rev. B **49**, 14251 (1994).
[36] G. Kresse and J. Furthmüller, Comput. Mater. Sci. **6**, 15 (1996).
[37] J. Perdew and Y. Wang, Phys. Rev. B **45**, 13244 (1992).
[38] P. E. Blöchl, Phys. Rev. B **50**, 17953 (1994).
[39] G. Kresse and D. Joubert, Phys. Rev. B **59**, 1758 (1999).
[40] S. H. Vosko, L. Wilk, and M. Nusair, Can. J. Phys. **58**, 1200 (1980).
[41] V. L. Moruzzi, P. M. Marcus, K. Schwarz, and P. Mohn, Phys. Rev. B **34**, 1784 (1986).
[42] S. S. Jaswal and J. Hafner, Phys. Rev. B **38**, 7311 (1988).
[43] M. D. Segall, R. Shah, C. J. Pickard, and M. C. Payne, Phys. Rev. B **54**, 16317 (1996).
[44] M. C. Payne, M. P. Teter, D. C. Allan, T. A. Arias, and J. D. Joannopoulos, Rev. Mod. Phys. **64**, 1045 (1992).
[45] S. J. Clark, M. D. Segall, C. J. Pickard, P. J. Hasnip, M. J. Probert, K. Refson, and M. C. Payne, Z. Kristallogr. **220**, 567 (2005).
[46] See EPAPS Document No. E-PRBMDO-79-024919 for details. For more information on EPAPS, see http://www.aip.org/pubservs/epaps.html.
[47] M. H. Lee, M. Ge, B. R. Sahu, P. Tarakeshwar, and K. S. Kim, J. Phys. Chem. B **107**, 9994 (2003).
[48] H. Häkkinen and U. Landman, Phys. Rev. B **62**, 2287 (2000).
[49] H. Häkkinen, M. Moseler, and U. Landman, Phys. Rev. Lett. **89**, 033410 (2002).
[50] L. Xiao and L. Wang, Chem. Phys. Lett. **392**, 452 (2004).
[51] R. M. Olson, S. Varganov, M. S. Gordon, H. Metiu, S. Chretien, P. Piecuch, K. Kowaleski, S. A. Kucharski, and M. Musia, J. Am. Chem. Soc. **127**, 1049 (2004).
[52] E. M. Fernandez, J. M. Soler, I. L. Garzon, and L. C. Balbás, Phys. Rev. B **70**, 165403 (2004).
[53] E. M. Fernandez, J. M. Soler, and L. C. Balbas, Phys. Rev. B **73**, 235433 (2006).
[54] W. Fa, C. Luo, and J. Dong, Phys. Rev. B **72**, 205428 (2005).
[55] A. J. Cox, J. G. Louderback, and L. A. Bloomfield, Phys. Rev. Lett. **71**, 923 (1993).
[56] A. J. Cox, J. G. Louderback, S. E. Apsel, and L. A. Bloomfield, Phys. Rev. B **49**, 12295 (1994).
[57] W. Zhang, Q. Ge, and L. Wang, J. Chem. Phys. **118**, 5793 (2003).
[58] B. Hammer and J. K. Nørskov, Adv. Catal. **45**, 71 (2000).